

Majorana zero modes in Y-shape interacting Kitaev wires

Bradraj Pandey,^{1,2} Nitin Kaushal,² Gonzalo Alvarez,³ and Elbio Dagotto^{1,2}

¹Department of Physics and Astronomy, The University of Tennessee, Knoxville, Tennessee 37996, USA

²Materials Science and Technology Division, Oak Ridge National Laboratory, Oak Ridge, Tennessee 37831, USA

³Computational Sciences and Engineering Division, Oak Ridge, Tennessee 37831, USA

(Dated: June 8, 2023)

Motivated by the recent experimental realization of minimal Kitaev chains using quantum dots, we investigate the Majorana zero modes (MZM) in Y-shape Kitaev wires. We solve the associated Kitaev models analytically at the sweet spot ($t_h = \Delta$) and derive the exact form of MZM wave-functions in this geometry. The novelty of our result is the observation of *non-local* MZMs near the junction center, made of a linear combination of edge sites MZMs for each arm. Furthermore, we simulate the stability of local (on site) and non-local MZMs modes in the presence of Coulomb repulsion, using density matrix renormalization group theory. Our local density-of-states calculation shows that these non-local MZMs are as equally topologically protected as the local MZMs when in the presence of Coulomb repulsion.

Introduction

Majorana zero modes (MZMs) are charge-neutral non-Abelian quasiparticles [1, 2]. They have attracted much interest because of their potential application in fault-tolerant topological quantum computing [2–5]. The occurrence of zero-bias peaks in tunneling spectroscopy is one of the experimental signatures of MZMs [6]. A promising platform to realize MZMs are semiconductor nanowires proximitized to superconductors, where MZMs are expected to develop at both ends of the wire [7]. Recently, the realization of MZMs was also proposed in quantum-dot-superconductor linear arrays [8–10]. These quantum-dots systems [11–16] are expected to overcome the problem of random-disorder potential, as compared to the proximitized semiconductor nanowires where the effect of disorder is strong [8] and may create false signal of MZMs in tunneling spectra [17]. Interestingly, the experimental realization of minimal Kitaev chain has been demonstrated using two quantum dots coupled through a short superconducting-semiconductor hybrid (InSb nanowire) [18]. In this experiment [18], two localized MZMs were observed in tunneling conductance measurements at the sweet spot $t_h = \Delta$.

In topological quantum computation, it is required to move and perform braiding operations of the MZMs [19, 20]. A strict 1D geometry is not sufficient to perform such braiding operations, because in 1D the MZMs can fuse during their exchange process [21, 22]. To realize non-Abelian statistics (or braiding), T and Y-shaped wires geometry have been proposed [19, 23, 24]. It has been shown that the MZMs in T-shape nanowires can be transformed under exchange, similarly to 2D $p + ip$ superconducting systems displaying non-Abelian statistics [19]. Braiding-based gates with MZMs using quantum dot arrays was proposed in Ref. [25].

This paper focuses on finding MZM modes near the junction of interacting Y-shaped Kitaev wires, which is important for all proposed multi-terminal nanowires and quantum-dots setups related to braiding and non-Abelian statistics of MZMs. In the context of proximity-induced semiconductor nanowires, there are only a few studies related to ground states of T-shaped wires [26, 27]. The sub-gap

properties of a three-terminal Josephson junction (composed of effective spinless p -wave superconductors), joined into a T-shaped normal-metallic region, has been studied using the scattering matrix approach in the non-interacting limit [27]. They found that depending upon the superconducting phase of each arm, the Majorana zero mode extended into the metallic region of either all three legs or two legs of the T-shape wire. However, in these studies the precise form of the Majorana wave functions and the effect of Coulomb interactions were not addressed [26, 27]. The repulsive Coulomb interaction is expected to suppress the pairing-induced bulk-gap and can affect the stability of Majorana modes [28, 29].

Motivated by the above described recent progress in realization of minimal Kitaev chain using quantum dots [18], we study the Majorana zero modes in Y-shaped interacting Kitaev wires. We address the question related to the exact form of Majorana wavefunctions near the junction and its dependency on the superconducting phases at each wire. Assuming each arm of Y-shape wire can take different values of superconducting (SC) phase [see Fig. 1a], we solve *exactly* the Kitaev model for Y-shapes wires working at the sweet spot $t_h = \Delta$. Remarkably, in terms of Majorana operators, we are able to write four independent commuting Hamiltonians, consisting of the three arms (I, II, III) and one central region (IV), as shown in Fig. 1b. This allow us to diagonalize the full system independently for each region and solve exactly at the sweet spot. We find the expected three localized MZMs on the edge sites of the Y-shape wire. Surprisingly, depending on the SC phase values, we also find exotic non-local MZMs near the central region, which are made from linear combinations of the local MZMs residing on the edge site of each arm.

Furthermore, we perform much needed unbiased simulations of the Majorana zero modes in Y-shaped interacting Kitaev wires, using density matrix renormalization group (DMRG) [30, 31]. In the non-interacting limit, we find peaks in the site-dependent local density-of-states (LDOS) at the locations predicted by our analytical calculations. In order to compare the stability of local vs. non-local MZMs, we examine the electron and hole components of the LDOS separately [32, 33], against the increase in repulsive Coulomb interactions. Interestingly, the $\text{LDOS}(\omega, j)$ calculations

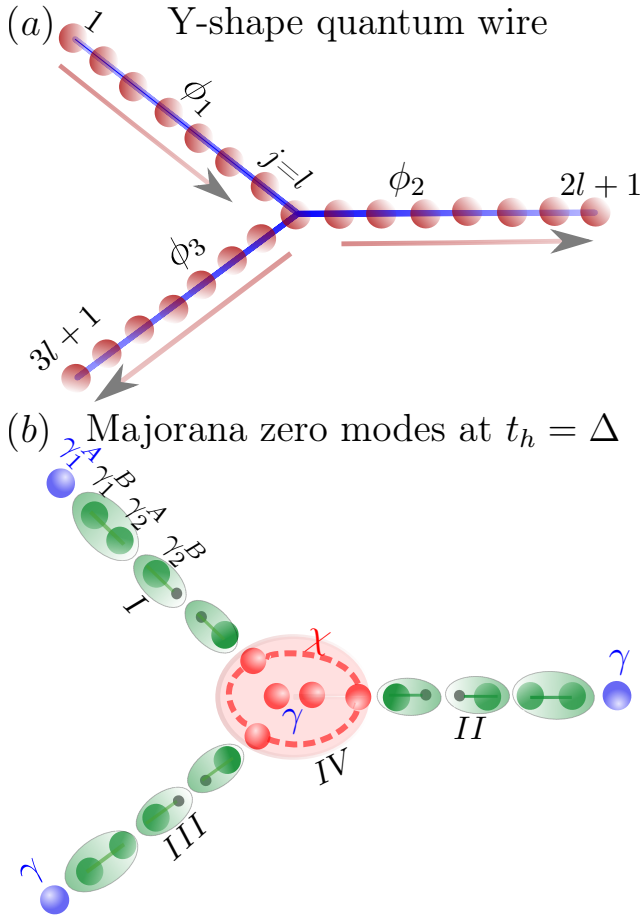


FIG. 1. (a) Schematic representation of the Y-shape Kitaev wires used here. ϕ_1 , ϕ_2 and ϕ_3 are the phases of the p -wave superconductor in each arm of the Y-shape wire. Arrows denote the directions of the pairing terms Δ and site index j in each wire. (b) Pictorial representation of the Majorana zero modes in the Y-shape Kitaev wire unveiled here, at $t_h = \Delta$. There are always three localized MZMs γ (blue color) at each end of the Y-shape wire. Depending upon the phases (ϕ_1 , ϕ_2 and ϕ_3) of each arm, near the center of the wire we observed exactly two situations: either (i) one non-local MZM (χ) or (ii) two non-local MZMs (χ) and one local MZM (γ). Green color MZMs form ordinary fermions at each bond.

indicate the non-local MZMs are as equally stable as the local-MZMs residing at the ends of the Y-shaped wire. We believe these MZMs should be observed in quantum-dots experiments, close to the sweet spots in the tunneling-conductance measurements [18]

Results

Description of analytical method

We solve the Y-shape Kitaev model analytically at the sweet spot $t_h = \Delta$ and $V = 0$, for three different sets of superconducting phases: (i) $\phi_1 = \pi$, $\phi_2 = 0$, and $\phi_3 = 0$, (ii) $\phi_1 = 0$, $\phi_2 = 0$, and $\phi_3 = 0$, and (iii) $\phi_1 = 0$, $\phi_2 = 0$, and $\phi_3 = \pi/2$. First, we divide the system Hamiltonian into

four different parts (for details see Model Hamiltonian) in terms of spinless fermionic operators. Then, we rewrite the system Hamiltonian in terms of Majorana operators, using the transformation $c_j = \frac{1}{\sqrt{2}}e^{-i\frac{\phi_j}{2}}(\gamma_j^A + i\gamma_j^B)$ [1]. In terms of the Majorana operators, remarkably the system can be written as four independent commuting Hamiltonians: (1) the three independent 1d wires (I, II, III) (see Fig. 1b) and (2) the central region (IV), consisting only of five Majorana operators (two from central site and three from edge sites of each leg), as shown in Fig. 1b. This procedure allows us to solve the Y-shape Kitaev model exactly at the sweet spot $t_h = \Delta$ and $V = 0$, for any values of the SC phases of each arm. For all three cases of SC phases discussed above, we find there is one Majorana zero mode at the outer edge of each arm (blue color in Fig. 1b), as expected intuitively. The novelty is that depending on the phase values of each arm, in addition to above mentioned outer edge MZMs, we find at the center region either (i) only one non-local MZM (χ) or (ii) two non-local MZMs (χ) accompanied with one local MZM (γ). These non-local MZMs (χ) are formed from the linear combinations of MZMs residing at the edge sites (near the central region) of each arm. These exotic non-local MZMs could be realized in quantum dot experiments, by changing the phases of each arm in a Y-shape geometry of quantum dots arrays.

In terms of Majorana operators, the Hamiltonian of each leg is independent of the SC phases (ϕ_1, ϕ_2, ϕ_3). Using the transformations $c_j^I = \frac{1}{\sqrt{2}}e^{-i\phi_1/2}(\gamma_{A,j}^I + i\gamma_{B,j}^I)$, $c_j^{II} = \frac{1}{\sqrt{2}}e^{-i\phi_2/2}(\gamma_{A,j}^{II} + i\gamma_{B,j}^{II})$ and $c_j^{III} = \frac{1}{\sqrt{2}}e^{-i\phi_3/2}(\gamma_{A,j}^{III} + i\gamma_{B,j}^{III})$, the Hamiltonian for the three legs H^I , H^{II} and H^{III} can be written in terms of Majorana operators as:

$$H^I = -2i\Delta \sum_{j=1}^{l-1} (\gamma_{A,j+1}^I \gamma_{B,j}^I), \quad (1)$$

$$H^{II} = -2i\Delta \sum_{j=l+2}^{2l} (\gamma_{A,j+1}^{II} \gamma_{B,j}^{II}), \quad (2)$$

$$H^{III} = -2i\Delta \sum_{j=2l+2}^{3l} (\gamma_{A,j+1}^{III} \gamma_{B,j}^{III}), \quad (3)$$

where we have used $t_h^x = t_h^y = |\Delta|$. In these equations, the Majorana operators $\gamma_{A,1}^I$, $\gamma_{B,2l+1}^{II}$, and $\gamma_{B,3l+1}^{III}$ are absent [19], and commute with these Hamiltonians, which indicates the presence of three end MZMs at the edge sites of the Y-shape Kitaev wire (see Fig. 1b), similarly as in the original Kitaev chain exact solution. For the central region, the Hamiltonian H^{IV} depends upon the SC phases. We solve H^{IV} for three different cases, in order to understand the nature of the central MZMs.

The case $\phi_1 = \pi$, $\phi_2 = 0$, and $\phi_3 = 0$

To explain the exact solution of Majorana wave functions in Y-shape geometries, we start with phase values $\phi_1 = \pi$,

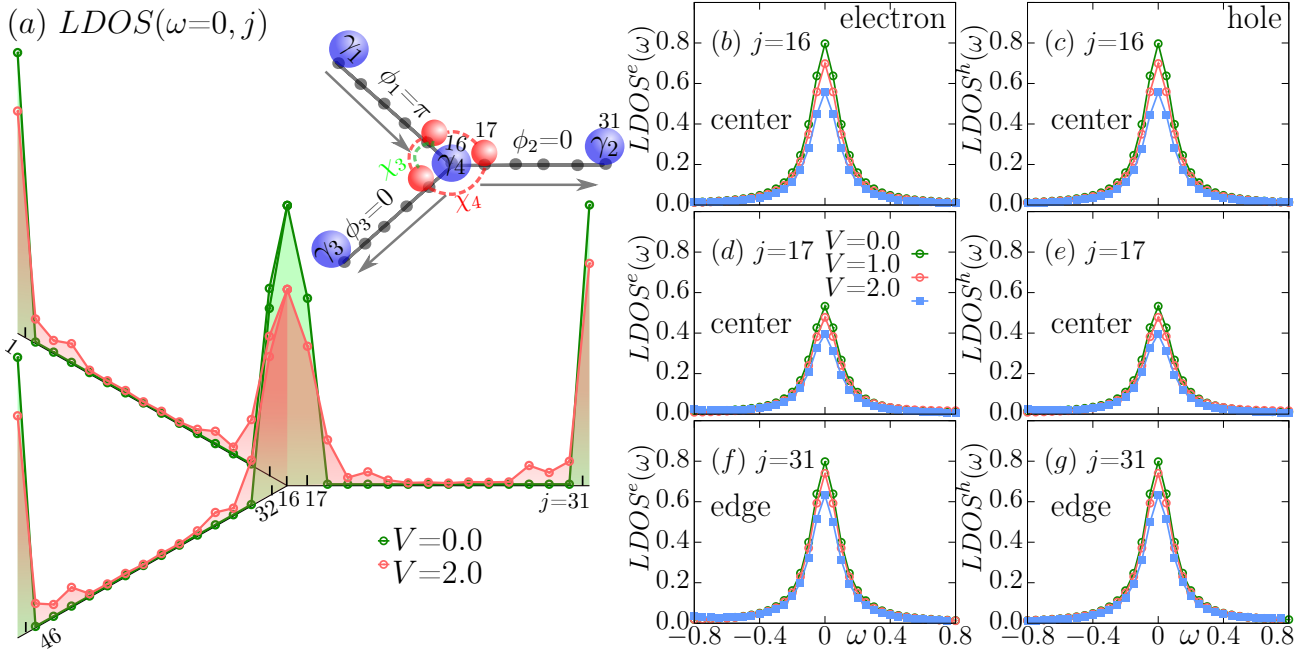


FIG. 2. Schematic representation of Majorana zero modes in a Y-shape Kitaev wire, for the case $\phi_1 = \pi$, $\phi_2 = 0$, and $\phi_3 = 0$, at $t_h = \Delta = 1$. (a) There are a total of six MZMs. For $V = 0$, three localized MZMs (γ_1 , γ_2 , and γ_3) at the edge sites $j = 1, 31, 46$ and in addition one localized MZM (γ_4) at the central site $j = 16$. Near this central region, there are two additional non-local Majoranas: χ_3 (distributed on sites $j = 15$ and 32) and χ_4 (distributed on sites $j = 15, 17$, and 32), which leads to a spectral weight $2/3$ (compared to the localized MZMs). At robust repulsion $V = 2$ the Majoranas remain exponentially localized over a few sites. The electron and hole parts of the LDOS(ω) vs. ω are shown for sites (b) $j = 1$, (d) $j = 17$, and (f) $j = 31$. For $V \leq 2$, the electron and hole parts of the LDOS(ω) are almost equal and shows peaks at $\omega = 0$, indicating the presence of stable MZMs on these sites.

$\phi_2 = 0$, and $\phi_3 = 0$ on arms *I*, *II*, and *III*, respectively. For these phase values, the pairing term at each arm preserves the rotational symmetry of the system, as under 120° rotation around the central sites $l + 1$, the system Hamiltonian remains invariant due to the π phase in arm *I* (see SM for more detail [34]) [35, 36].

For the central sites, using the relations $c_l = \frac{1}{\sqrt{2}}e^{-i\phi_1/2}(\gamma_{A,l}^I + i\gamma_{B,l}^I)$, $c_{l+1} = \frac{1}{\sqrt{2}}(\gamma_{A,l+1}^{IV} + i\gamma_{B,l+1}^{IV})$, $c_{l+2} = \frac{1}{\sqrt{2}}e^{-i\phi_2/2}(\gamma_{A,l+2}^{II} + i\gamma_{B,l+2}^{II})$, and $c_{2l+2} = \frac{1}{\sqrt{2}}e^{-i\phi_3/2}(\gamma_{A,2l+2}^{III} + i\gamma_{B,2l+2}^{III})$, the sector H^{IV} (with $\phi_1 = \pi$, $\phi_2 = 0$, and $\phi_3 = 0$) can be transformed in terms of Majorana operators as:

$$H^{IV} = -2i\Delta \left(\gamma_{B,l}^I + \gamma_{A,l+2}^{II} + \gamma_{A,2l+2}^{III} \right) \gamma_{B,l+1}^{IV}. \quad (4)$$

Note that in Eq. 4 the Majorana operator $\gamma_{A,l+1}^{IV}$ at the central site $l + 1$ is absent, signaling the presence of a localized MZM at site $j = 16$. Next, we write Eq. 4 in terms of a 4×4 matrix in the basis of $(\gamma_{B,l}^I, \gamma_{A,l+2}^{II}, \gamma_{A,2l+2}^{III}, \gamma_{B,l+1}^{IV})$ and obtained four eigenvalues $(-\sqrt{3}, \sqrt{3}, 0, 0)$. The last two eigenvalues (e_3, e_4) take value zero, and the associated eigenvectors $\chi_3 = -\frac{1}{\sqrt{2}}\gamma_{B,l}^I + \frac{1}{\sqrt{2}}\gamma_{A,2l+2}^{III}$ and $\chi_4 = -\frac{1}{\sqrt{6}}\gamma_{B,l}^I + \sqrt{\frac{2}{3}}\gamma_{A,l+2}^{II} - \frac{1}{\sqrt{6}}\gamma_{A,2l+2}^{III}$, develop with properties $\chi_3 = \chi_3^\dagger$ and $\chi_4 = \chi_4^\dagger$. In addition, χ_3 and χ_4 also commute with H^{IV} ; these properties

confirm the presence of two non-local MZMs in the central region. These two non-local MZMs, χ_3 and χ_4 , are made from linear combinations of MZMs on the edge sites of the arms (see Fig. 2a). The diagonalized Hamiltonian for the central site can be written as

$$H^{IV} = 2\sqrt{3}\Delta \left(\bar{\chi}_2 \chi_2 - \frac{1}{2} \right), \quad (5)$$

where $\chi_2 = \frac{i}{\sqrt{6}}\gamma_{B,l}^I + \frac{i}{\sqrt{6}}\gamma_{A,l+2}^{II} + \frac{i}{\sqrt{6}}\gamma_{A,2l+2}^{III} + \frac{1}{\sqrt{2}}\gamma_{B,l+1}^{IV}$ is an ordinary fermion.

The other remaining Hamiltonians for each arm can be diagonalized using fermionic operators $d_{k,j} = \frac{1}{\sqrt{2}}(\gamma_{B,j}^k + i\gamma_{A,j+1}^k)$, where $k = I, II$, or *III*. The diagonalized Hamiltonian H^I , H^{II} , and H^{III} are:

$$H^I = 2\Delta \sum_{j=1}^{l-1} \left(d_{I,j}^\dagger d_{I,j} - \frac{1}{2} \right), \quad (6)$$

$$H^{II} = 2\Delta \sum_{j=l+2}^{2l} \left(d_{II,j}^\dagger d_{II,j} - \frac{1}{2} \right), \quad (7)$$

$$H^{III} = 2\Delta \sum_{j=2l+2}^{3l} \left(d_{III,j}^\dagger d_{III,j} - \frac{1}{2} \right). \quad (8)$$

In conclusion, our analytical calculations predict a total of six MZMs, for the case of $\phi_1 = \pi$, $\phi_2 = 0$ and $\phi_3 = 0$. These six MZMs leads to eight fold-degeneracy in the ground state of the system [4], which we also find is fully consistent with our numerical Lanczos calculations (see SM for more details [34]).

Next, we analyze the stability of MZMs in the presence of a nearest-neighbor interaction $H_I = Vn_jn_{j+1}$. We calculate the LDOS, using DMRG for a Y-shaped geometry with system size $L = 46$. As shown in Fig. 2a, the site dependent LDOS($\omega = 0, j$) shows sharp peaks for the edge sites $j = 1, 31$, and 46 , indicating three localized MZMs at each edge of the arms. At the central site $l + 1$, there is a sharp peak with same height as for the edge sites, showing the presence of a localized MZM γ_4 at site $j = 16$, as already discussed. Interestingly, there are three other peaks in that LDOS($\omega = 0, j$) on sites $j = 15, 17$, and 32 , with height $2/3$ as compared to the edge sites. These three peaks signal the presence of two non-local MZMs, distributed over three central sites ($j = 15, 17$, and 32). With increase in interaction to $V = 2$, the Majoranas are no longer strictly localized on a single site j . The MZMs are still exponentially decaying over a few more sites and consequently the peak height of LDOS($\omega = 0, j$) decreases (Fig. 2a). This shows that the Majorana zero modes are topologically protected against moderate values of Coulomb interaction.

To compare the topological protection against V , for local and non-local MZMs, we calculate the electron and hole parts of LDOS(ω, j) separately for the edge and central sites (right panel of Fig. 2). In Fig. 2b and c, we show the electron and hole part of LDOS(ω, j) for the central site $j = 16$. The peak height of electron and hole parts of LDOS(ω) at $\omega = 0$ decrease to the same values with increasing V , showing the preservation of its MZM nature ($\gamma = \gamma^\dagger$) [33]. Due to the rotational symmetry of the system, sites near the center $j = 15, 17$, and 32 are equivalent and they behave very similarly increasing V . In Fig. 1(d) and (e), we show the electron and hole parts of LDOS(ω, j) for site $j = 17$. As discussed previously, the two non-local MZMs χ_3 and χ_4 are distributed on sites ($j = 15$ and 32) and ($j = 15, 17$, and 32), with total amplitude $2/3$ on each site ($j = 15, 17$, and 32), which leads to a spectral weight $2/3$ (compared to the localized MZMs) in the LDOS(ω, j) for site $j = 17$ (also for $j = 15$ and 32 at $V = 0$). Figures 2(f) and (g) present electron and hole part of LDOS(ω, j) for the edge site $j = 31$ with increasing V (note: sites $j = 1$ and 46 are equivalent). The rate of decrease in peak height in electron and hole part of LDOS(ω, j), for non-local MZMs at site $j = 17$ and local MZM at edge site $j = 31$ are almost identical when increasing V ($V \leq 2$). The LDOS(ω, j) of the local MZM at the central site $j = 16$ decreases with a slightly faster rate because it has a finite overlap with χ_3 and χ_4 , with increasing V .

The case $\phi_1 = 0, \phi_2 = 0$, and $\phi_3 = 0$

Here, we consider the Y-shape geometry with the same phase $\phi = 0$ on each arm. Surprisingly, for $\phi_1 = 0, \phi_2 = 0$, and $\phi_3 = 0$, the pairing term in the Hamiltonian breaks the rotational symmetry, as after 120° anti-clockwise rotation

around the central sites $l + 1$, the pairing term in leg I changes its sign (becomes negative due fermionic anticommutations) [see also SM for details [34]]. The arm II and arm III have reflection symmetry around the central site $l + 1$. Using the same transformations as discussed previously, the H^I , H^{II} and H^{III} of each arm in terms of Majorana operators can be written in similar form as described by Eqs. 1, 2, and 3. Again, in these equations, the Majorana operators $\gamma_{A,1}^I$, $\gamma_{B,2l+1}^{II}$, and $\gamma_{B,3l+1}^{III}$ are absent, indicating the presence of three edge MZMs on sites $j = 1, 31$, and 46 . The Hamiltonian for the central region H^{IV} can be transformed as:

$$H^{IV} = -2i\Delta \left[\gamma_{A,l+1}^{IV} \gamma_{B,l}^I + \left(\gamma_{A,l+2}^{II} + \gamma_{A,2l+2}^{III} \right) \gamma_{B,l+1}^{IV} \right].$$

In the above equation, H^{IV} has a reflection symmetry [$\gamma_{A,l+2}^{II} \leftrightarrow \gamma_{A,2l+2}^{III}$]. Thus, defining the operators

$$\begin{aligned} R_1 &= \frac{1}{\sqrt{2}} \left(\gamma_{A,l+2}^{II} + \gamma_{A,2l+2}^{III} \right), \\ R_2 &= \frac{1}{\sqrt{2}} \left(\gamma_{A,l+2}^{II} - \gamma_{A,2l+2}^{III} \right) \end{aligned} \quad (9)$$

the Hamiltonian H^{IV} further simplifies as

$$H^{IV} = -2i\Delta \gamma_{A,l+1}^{IV} \gamma_{B,l}^I - 2\sqrt{2}i\Delta R_1 \gamma_{B,l+1}^{IV}. \quad (10)$$

In Eq. 10 the operator R_2 is absent and has the properties $R_2 = R_2^\dagger$, and $[H^{IV}, R_2] = 0$, indicating R_2 is a Majorana zero mode. The Majorana zero mode $R_2 = \frac{1}{\sqrt{2}} \left(\gamma_{A,l+2}^{II} - \gamma_{A,2l+2}^{III} \right)$ is equally distributed on sites 17 (II leg) and 32 (III leg) (see Fig. 3a), showing that R_2 is indeed a non-local MZM. Next, we write Eq. 10 in terms of a 4×4 matrix in the basis of $\left[\gamma_{A,l+1}^{IV}, R_1, \gamma_{B,l+1}^{IV}, \gamma_{B,l}^I \right]$ and obtain four eigenvalues $(-\sqrt{2}, \sqrt{2}, -1, 1)$. The central region diagonal Hamiltonian can be written in terms of ordinary fermions χ_2 and χ_4 as

$$H^{IV} = 2\sqrt{2}\Delta \left(\bar{\chi}_2 \chi_2 - \frac{1}{2} \right) + 2\Delta \left(\bar{\chi}_4 \chi_4 - \frac{1}{2} \right), \quad (11)$$

with $\chi_2 = \frac{1}{\sqrt{2}} \left(iR_1 + \gamma_{B,l+1}^{IV} \right)$ and $\chi_4 = \frac{1}{\sqrt{2}} \left(i\gamma_{B,l+1}^{IV} + \gamma_{B,l}^I \right)$ (see SM for more detail [34]). The diagonalized Hamiltonian H^I , H^{II} , and H^{III} takes similar form as Eqs. 6, 7, and 8, in terms of the ordinary $d_{k,j}$ fermionic operators. In summary, our analytical calculation finds a total of four MZMs (three localized at the edge sites and one non-local MZM near the center region). These four MZMs results in four-fold degeneracy in the ground state of the system, which is also consistent with our full-diagonalization numerical results.

Figure 3 shows DMRG results for $L = 46$ sites at $t_h = \Delta$ and for different values of the Coulomb interaction V . At $V = 0$, the site dependent LDOS($\omega = 0, j$) shows sharp localized peaks at the edge sites $j = 1, 31$, and 46 , indicating three localized MZMs on those edge sites, as expected. Near

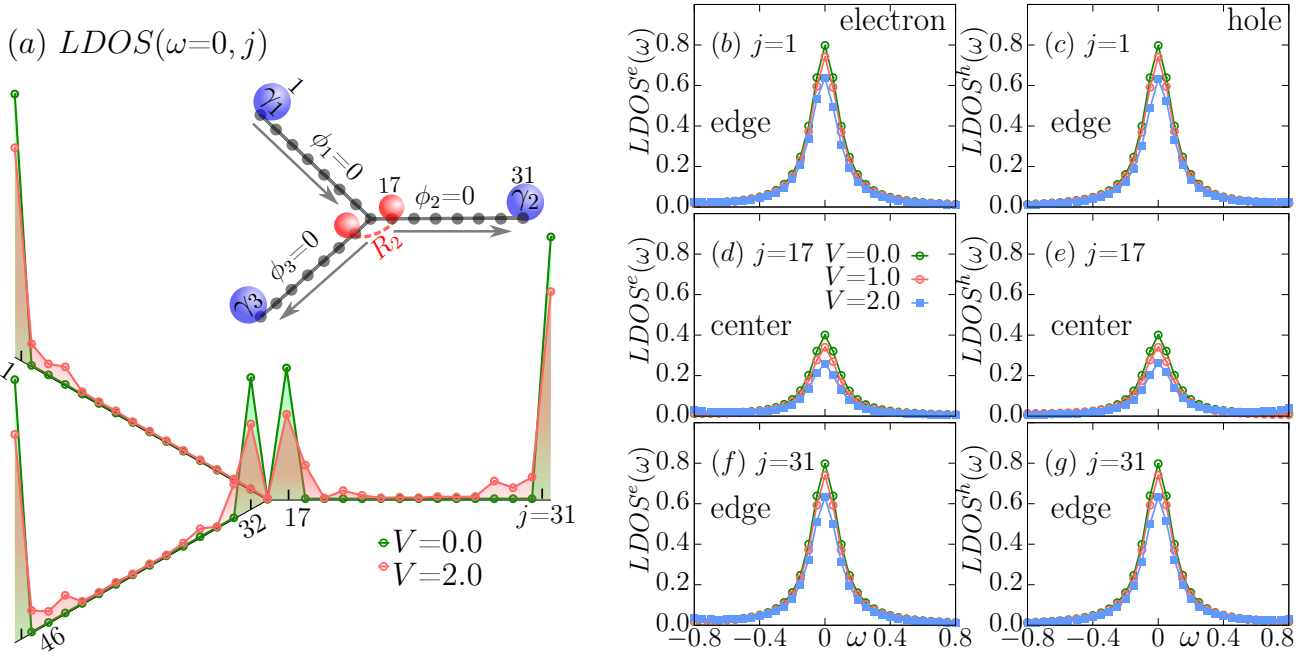


FIG. 3. Schematic representation of Majorana zero modes in a Y-shape Kitaev wire, with $\phi_1 = 0$, $\phi_2 = 0$, and $\phi_3 = 0$, and at $t_h = \Delta = 1$. (a) In this case, there are a total of four MZMs. Three are localized at the end sites $j = 1, 31$, and 46 . Near the central region, there is one extra non-local MZM χ_4 . The non local MZM R_2 is equally distributed among the central sites $j = 17$ and 32 , leading to an spectral weight $1/2$ (compared to the localized MZMs) as shown in the $LDOS(\omega = 0, j)$ on these central sites. For $V = 2$ the MZMs are spread over a few sites compared to the $V = 0$ case. The electron and hole parts of the $LDOS(\omega)$ vs. ω are shown for sites (b) $j = 1$, (d) $j = 17$, and (f) $j = 31$. For $V \leq 2$ the electron and hole parts of the $LDOS(\omega)$ are almost equal and shows peaks at $\omega = 0$, indicating the presence of stable MZMs on sites $j = 1, 17, 31, 32$, and 46 . Note the weight at $j = 17$ is half that of sites $j = 1$ and $j = 31$.

the center, the $LDOS(\omega = 0, j)$ displays two peaks at sites $j = 17$ and 32 , with height $1/2$ compared to the edge sites, suggesting the presence of a non-local MZM. With increase in interaction ($V = 2$), these MZMs remain exponentially localized over a few sites (Fig. 3a). To compare the stability of local and non-local MZMs, we calculate the electron and hole parts of $LDOS(\omega, j)$ for different values V . The peak values for $LDOS^e(\omega)$ (Fig. 3b and f) and $LDOS^h(\omega)$ (Fig. 3c and g) at $\omega = 0$, for edge sites $j = 1$ and 31 , decrease to the same values with increase in V . This shows that the characteristic features of the local MZM remain and the spectral weight of electron and hole part of $LDOS(\omega, j)$ are equal [33], at moderate values of $V \leq 2$. Interestingly, the spectral weight of electron and hole of $LDOS(\omega)$ for site $j = 17$, takes value half (compared to the local MZMs on edge sites) at $V = 0$. This is because the non-local MZM $R_2 = \frac{1}{\sqrt{2}} (\gamma_{A,17}^{II} - \gamma_{A,32}^{III})$ is equally distributed at sites $j = 17$ and 32 . Increasing the repulsion strength V , the peak values of $LDOS^e(\omega)$ (Fig. 3d) and $LDOS^h(\omega)$ (Fig. 3e) are reduced (but still take the same values). The rate of decrease in peak height for local and non-local MZMs are almost the same, which shows these Majorana modes are equally topologically protected against V .

The case $\phi_1 = 0, \phi_2 = 0$, and $\phi_3 = \pi/2$

Finally, we consider the Y-shape Kitaev wires with phases $\phi_1 = 0, \phi_2 = 0$, and $\phi_3 = \pi/2$. This limit is also equivalent

to two perpendicular Kitaev chains with phase difference of $\pi/2$ (T-shape wire) [19, 37]. The Hamiltonian for three legs H^I, H^{II} , and H^{III} takes the same form as Eqs. 1, 2, and 3, in terms of Majorana operators. As expected, in these equations the Majorana operators $\gamma_{A,l}^I, \gamma_{B,2l+1}^{II}$, and $\gamma_{B,3l+1}^{III}$ are absent, indicating the presence of three end MZMs at the edge sites of the Y-shape Kitaev wire (see Fig. 4). The central region, H^{IV} , in terms of Majorana operators becomes:

$$H^{IV} = -\sqrt{2}i\Delta\gamma_{A,2l+2}^{III}(\gamma_{A,l+1}^{IV} + \gamma_{B,l+1}^{IV}) - 2i\Delta(\gamma_{A,l+1}^{IV}\gamma_{B,l}^I + \gamma_{A,l+2}^{II}\gamma_{B,l+1}^{IV}). \quad (12)$$

Equation 12 can be written as a 5×5 matrix in the basis $[\gamma_{A,l+2}^{II}, \gamma_{A,2l+2}^{III}, \gamma_{B,l}^I, \gamma_{A,l+1}^{IV}, \gamma_{B,l+1}^{IV}]$. After diagonalizing H^{IV} , we obtained five eigenvalues $(-\sqrt{2}, \sqrt{2}, -1, 1, 0)$. The last eigenvalue $e_5 = 0$ and its eigenvector $\chi_5 = -\frac{1}{2}\gamma_{A,l+2}^{II} + \frac{1}{\sqrt{2}}\gamma_{A,2l+2}^{III} + \frac{1}{2}\gamma_{B,l}^I$ has the property $\chi_5 = \chi_5^\dagger$, and $[H^{IV}, \chi_5] = 0$, confirming the presence of a non-local MZM near the junction. The non-local MZM χ_5 is made from linear combinations of local MZMs residing at sites $j = 15, 17$, and 32 (see Fig. 4). The central region H^{IV} can be written in diagonal form as:

$$H^{IV} = 2\sqrt{2}\Delta\left(\bar{\chi}_2\chi_2 - \frac{1}{2}\right) + 2\Delta\left(\bar{\chi}_4\chi_4 - \frac{1}{2}\right), \quad (13)$$

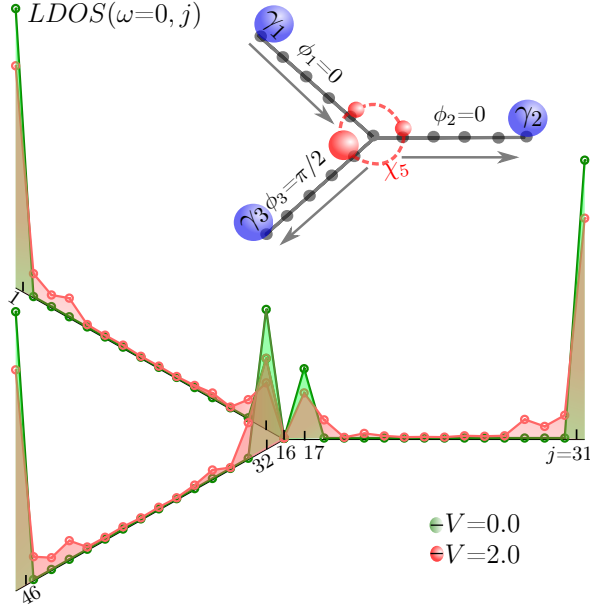


FIG. 4. Schematic representation of Majorana zero modes in the Y-shape Kitaev wire with $\phi_1 = 0$, $\phi_2 = 0$, and $\phi_3 = \pi/2$, and at $t_h = \Delta = 1$. The LDOS($\omega = 0, j$) shows four Majorana zero modes: (i) three localized MZMs at the end sites $j = 1, 31$, and 46 , while (ii) near the central region, there is one non-local Majorana χ_4 . For $V = 0$, the MZM χ_5 is distributed among the central sites $j = 15, 17$, and 32 , with spectral weight $1/4, 1/4$, and $1/2$, respectively (compared to localized MZMs). For $V = 2$ the MZMs are spread over a few sites compared to the $V = 0$ case.

where $\chi_2 = \frac{i}{2\sqrt{2}}\gamma_{A,l+2}^{II} + \frac{i}{2}\gamma_{A,2l+2}^{III} - \frac{i}{2\sqrt{2}}\gamma_{B,l}^I + \frac{1}{2}\gamma_{A,l+1}^{IV} + \frac{1}{2}\gamma_{B,l+1}^{IV}$ and $\chi_4 = \frac{i}{2}\gamma_{A,l+2}^{II} + \frac{i}{2}\gamma_{B,l}^I - \frac{1}{2}\gamma_{A,l+1}^{IV} + \frac{1}{2}\gamma_{B,l+1}^{IV}$. Note that the diagonalized system Hamiltonian, in case of the SC phase ($\phi_1 = 0, \phi_2 = 0$, and $\phi_3 = \pi/2$) and ($\phi_1 = 0, \phi_2 = 0$, and $\phi_3 = 0$) take similar form [see Eqs. 11 and 13], which lead to the same energy spectrum for both cases, although the form of non-local Majoranas wavefunctions are quite different for these two cases. The remaining Hamiltonians H^I, H^{II} , and H^{III} , after diagonalizing in terms of the ordinary $d_{k,j}$ fermionic operators, take similar forms as Eqs. 6, 7, and 8. In conclusion, our analytical calculations find a total of 4 MZMs. The three local MZMs are located at edge sites in their natural positions, while a non-local MZM χ_5 is situated near the central region. These four MZMs results in four-fold degeneracy in the ground state of the system.

In Fig. 4, we present the DMRG calculations with $\phi_1 = 0$, $\phi_2 = 0$, and $\phi_3 = \pi/2$ for different values of V using a system size $L = 46$. Similarly to the previous cases, the LDOS($\omega = 0, j$) shows sharp peaks for the edge sites $j = 1, 31$, and 46 , indicating three localized edge MZMs. Interestingly, near the center LDOS($\omega = 0, j$) shows three peaks with heights $1/4, 1/4$, and $1/2$ (compared to the edge sites) on sites $j = 15, 17$, and 32 , respectively. These peaks in LDOS($\omega = 0, j$) indicates the presence of a non-local MZM near the central site. The peak height can be explained

by the special form of the non-local MZM wavefunction $\chi_5 = -\frac{1}{2}\gamma_{A,l+2}^{II} + \frac{1}{2}\gamma_{B,l}^I + \frac{1}{\sqrt{2}}\gamma_{A,2l+2}^{III}$, showing that χ_5 is distributed on sites $j = 15, 17$, and 32 with amplitudes $1/4, 1/4$, and $1/2$, respectively. Increasing the repulsion V , the peak height of LDOS($\omega = 0, j$) decreases for different sites and these MZMs are exponentially localized over a few sites (Fig. 4). We find that the peak height of the electron and hole part of LDOS($\omega = 0, j$) take the same values even for $V = 2$, indicating the MZMs are quite stable against repulsive interaction for $V \leq 2$.

Discussion

In this publication, we studied the Y-shaped interacting Kitaev chains using analytical and DMRG methods for different superconducting phases at each arm. At the sweet spot $t_h = \Delta$ and $V = 0$, we show the system can be divided into four independent Hamiltonians (three arms and one central region) when using the Majorana degrees of freedom. We found exact analytical solutions at the sweet spot and predict the exact form of Majorana wavefunctions for different sets of SC phases of each arm. Remarkably, the central region can be written in terms of just five Majorana operators, and we thus unveil the non-local nature of these MZMs. Based on our analytical and DMRG results: (i) For $\phi_1 = \pi, \phi_2 = 0$, and $\phi_3 = 0$, we predict a total of six MZMs. There are three local MZMs on each edge sites, one local MZM at the central site, and also there are two non-local MZMs near the central region, which results in three peaks at sites l (arm I), $l + 1$ (arm II), and $2l + 2$ (arm III), with heights $2/3$ (as compared to the edge sites), in the site-dependent LDOS calculations. (ii) For $\phi_1 = 0, \phi_2 = 0$, and $\phi_3 = 0$, we find a total of four MZMs, three localized at the edge sites and one non-local MZM near the central site. The non-local MZM is equally distributed on site $l + 2$ (arm II) and $2l + 2$ (arm III), leading to two peaks with height $1/2$ (compared to the edge sites) as unveiled by the site-dependent LDOS. (iii) For $\phi_1 = 0, \phi_2 = 0$, and $\phi_3 = \pi/2$, we find a total of four MZMs. As expected three localized on the edge sites and one non-local MZM near the center. The non-local MZM is distributed on sites l (arm I), $l + 2$ (arm II), and $2l + 2$ (arm III), which leads to three peaks with heights $1/4, 1/4$, and $1/2$ in the LDOS calculation. Furthermore, we compare the stability of local and non-local MZMs against the repulsive interaction V , by calculating the electron and hole part of LDOS(ω, j) separately. Our DMRG results shows the local and non-local MZMs are equally stable, as the peak values of LDOS(ω, j) reduce with similar rate, for moderate values of repulsive interaction. We believe our proposed exotic non-local MZMs could be realized in quantum-dot systems [18] at the sweet spot, using just seven quantum dots in Y-shape geometry.

In this paper, we primarily focused on finding the physical location of the MZMs in a Y-shape geometry Kitaev chain. In the near future, it will be also interesting to study MZMs in the X-shaped Kitaev wire, using similar analytical and DMRG methods. A recent study shows the X-shape wire is also quite important for the braiding process in quantum wires [38, 39].

Methods

Model Hamiltonian

The Hamiltonian for the Y-shaped Kitaev model at the sweet spot $t_h = \Delta$, with superconducting phases ϕ_1 , ϕ_2 , and ϕ_3 , at each arm, can be divided into four different parts. The Hamiltonian for each leg can be written as:

$$H^I = \sum_{j=1}^{l-1} \left(-t_h^x c_j^\dagger c_{j+1} + e^{i\phi_1} \Delta c_j c_{j+1} + H.c. \right), \quad (14)$$

$$H^{II} = \sum_{j=l+2}^{2l} \left(-t_h^x c_j^\dagger c_{j+1} + e^{i\phi_2} \Delta c_j c_{j+1} + H.c. \right), \quad (15)$$

$$H^{III} = \sum_{j=2l+2}^{3l} \left(-t_h^y c_j^\dagger c_{j+1} + e^{i\phi_3} \Delta c_j c_{j+1} + H.c. \right). \quad (16)$$

Moreover, the Hamiltonian for the central site $l+1$ joining each leg edge site can be written as:

$$H^{IV} = \left(-t_h^x c_l^\dagger c_{l+1} + e^{i\phi_1} \Delta c_l c_{l+1} + H.c. \right) \\ \left(-t_h^x c_{l+1}^\dagger c_{l+2} + e^{i\phi_2} \Delta c_{l+1} c_{l+2} + H.c. \right) \\ \left(-t_h^y c_{l+1}^\dagger c_{2l+2} + e^{i\phi_3} \Delta c_{l+1} c_{2l+2} + H.c. \right). \quad (17)$$

DMRG method

In order to solve numerically, the Y-shaped Kitaev Hamiltonian and measure observables, we have used the density matrix renormalization group (DMRG) method [40, 41] with DMRG++ [30]. We performed our DMRG calculations within the two-site DMRG approach, for a system size $L = 46$ sites and employing $m = 1500$ states, with truncation error $\leq 10^{-10}$.

Local density-of-states

We have calculated the local density-of-states $LDOS(\omega, j)$ as a function of frequency ω and site j , Krylov-space correction vector DMRG; for a technical review see [31]. The electron part of the LDOS(ω, j) is [33]:

$$LDOS^e(\omega, j) = \frac{1}{\pi} \text{Im} \left[\left\langle \psi_0 \left| c_j^\dagger \frac{1}{\omega + H - (E_g - i\eta)} c_j \right| \psi_0 \right\rangle \right], \quad (18)$$

and the hole part of LDOS(ω, j) is [33]:

$$LDOS^h(\omega) = \frac{-1}{\pi} \text{Im} \left[\left\langle \psi_0 \left| c_j \frac{1}{\omega - H + (E_g - i\eta)} c_j^\dagger \right| \psi_0 \right\rangle \right], \quad (19)$$

where c_i is the fermionic annihilation operator while c_j^\dagger is the creation operator, E_g is the ground state energy. We use as broadening parameter the value $\eta = 0.1$ as in previous studies [21, 42]. The total local density-of-states is defined as $LDOS(\omega, j) = LDOS^e(\omega, j) + LDOS^h(\omega, j)$. For the Majorana zero mode, it is expected that the peak values of $LDOS^e(\omega, j)$ and $LDOS^h(\omega, j)$ be close to $\omega = 0$.

Data availability

The data that support the findings of this study are available from the corresponding author upon request.

Code availability

The computer codes used in this study are available at <https://github.com/g1257/dmrgPlusPlus/>.

Acknowledgments

The work of B.P., N.K., and E.D. was supported by the U.S. Department of Energy (DOE), Office of Science, Basic Energy Sciences (BES), Materials Sciences and Engineering Division. G. A. was supported by the U.S. Department of Energy, Office of Science, National Quantum Information Science Research Centers, Quantum Science Center.

Author contributions

B.P. and E.D. designed the project. N.K. and B.P. carried out the analytical calculations for the Y-shaped Kitaev model. B.P. performed the numerical DMRG calculations. G.A. developed the DMRG++ computer program. B.P., N.K., and E.D. wrote the manuscript. All co-authors provided useful comments and discussion on the paper.

Competing interests

The authors declare no competing interests.

Additional information

Correspondence should be addressed to Bradraj Pandey (bradraj.pandey@gmail.com).

- [1] Kitaev AY. Unpaired Majorana fermions in quantum wires. *Phys.-Usp.* **44**, 131 (2001).
- [2] Kitaev AY. Fault-tolerant quantum computation by anyons. *Ann Phys (NY)* **303**, 2 (2003).
- [3] Sarma, S., Freedman, M. Nayak, C. Majorana zero modes and topological quantum computation. *npj Quantum Inf* **1**, 15001 (2015).
- [4] Nayak C, Simon SH, Stern A, Freedman M, Sarma SD.

Non-abelian anyons and topological quantum computation. *Rev Mod Phys* **80**, 1083 (2008).

- [5] Scheurer, M. S., & Shnirman. Nonadiabatic processes in Majorana qubit systems. *Phys. Rev. B* **88**, 064515 (2013).
- [6] Law, K. T., Lee, P. A., and Ng, T. K. Majorana Fermion Induced Resonant Andreev Reflection. *Phys. Rev. Lett.* **103**, 237001 (2009).
- [7] Lutchyn, R. M., Sau, J. D., Das Sarma S. Majorana

- fermions and a topological phase transition in semiconductor–superconductor heterostructures. *Phys. Rev. Lett.* **105**, 077001 (2010).
- [8] Sau, J., Sarma, S. Realizing a robust practical Majorana chain in a quantum-dot-superconductor linear array. *Nat Commun.* **3**, 964 (2012).
- [9] Tsintzis, A., Souto, R. S., Leijnse, M. Creating and detecting poor man’s Majorana bound states in interacting quantum dots. *Phys. Rev. B.* **106**, L201404 (2022).
- [10] Mills, A.R., Zajac, D.M., Gullans, M.J. et al. Shuttling a single charge across a one-dimensional array of silicon quantum dots. *Nat Commun.* **10**, 1063 (2019).
- [11] Leijnse, M. and Flensberg, K. Introduction to topological superconductivity and Majorana fermions. *Semicond. Sci. Technol.* **27**, 124003 (2012).
- [12] Górski, G., Barański, J., Weymann, I. et al. Interplay between correlations and Majorana mode in proximitized quantum dot. *Sci Rep.* **8**, 15717 (2018)
- [13] Hofstetter, L., Csonka, S., Nygård, J. et al. Cooper pair splitter realized in a two-quantum-dot Y-junction. *Nature.* **461**, 960–963 (2009).
- [14] Deng, M. T., Vaitiekėnas, E., Hansen, E. B., Danon, J. et al. Majorana bound state in a coupled quantum-dot hybrid-nanowire system. *Science* **354**, 1557–1562 (2016).
- [15] Liu, C.-X., Wang, G., Dvir, T. & Wimmer, M. Tunable superconducting coupling of quantum dots via Andreev bound states in semiconductor-superconductor nanowires. *Phys. Rev. Lett.* **129** 267701 (2022)
- [16] Rančić, J. M., Hoffman, S., Schrade, C., Klinovaja, J., & Loss, D. Entangling spins in double quantum dots and Majorana bound states. *Phys. Rev. B.* **99** 165306 (2019)
- [17] Stanescu, T. D., Lutchyn, R. M. & Das Sarma, S. Majorana fermions in semiconductor nanowires. *Phys. Rev. B.* **84**, 144522 (2011).
- [18] Dvir, T., Wang, G., van Loo, N. et al. Realization of a minimal Kitaev chain in coupled quantum dots. *Nature* . **614**, 445–450 (2023).
- [19] Alicea, J., Oreg, Y., Refael, G. et al. Non-Abelian statistics and topological quantum information processing in 1D wire networks. *Nature Phys.* **7**, 412–417 (2011).
- [20] Aasen, D., Hell, M., Mishmash, R. V., Higginbotham, A., et al. Milestones toward Majorana-based quantum computing. *Phys. Rev. X.* **6**, 031016 (2016).
- [21] Pandey, B., Mohanta, N., Dagotto, E. Out-of-equilibrium Majorana zero modes in interacting Kitaev chains. *Phys. Rev. B.* **107**, L060304 (2023).
- [22] Zhou, T., Dartailh, M.C., Sardashti, K., Han, J. E. et al. Fusion of Majorana bound states with mini-gate control in two-dimensional systems. *Nat Commun.* **13**, 1738 (2022).
- [23] van Heck, B., Akhmerov, A. R., Hassler, F., Burrello, M. Beenakker, C. W. J. Coulomb-assisted braiding of majorana fermions in a josephson junction array. *New J. Phys.* **14**, 035019 (2012).
- [24] Harper, F., Pushp, A., Roy, R. Majorana braiding in realistic nanowire Y-junctions and tuning forks. *Phys. Rev. Research.* **1**, 033207 (2019).
- [25] Boross, P., Pályi, A. Braiding-based quantum control of a Majorana qubit built from quantum dots. *arXiv:2305.08464*. (2023).
- [26] Y Zhou and M W Wu. Majorana fermions in T-shaped semiconductor nanostructures. *J. Phys.: Condens. Matter* . **26**, 065801 (2014).
- [27] Spånslätt, C., Ardonne, E. Extended Majorana zero modes in a topological superconducting-normal T-junction. *J. Phys.: Condens. Matter* . **29**, 105602 (2017).
- [28] Stoudenmire, E. M., Alicea, J., Starykh, O. A., and Fisher, M. P. A. Interaction effects in topological superconducting wires supporting Majorana fermions. *Phys. Rev. B.* **84**, 014503 (2011).
- [29] Tsintzis, A., Souto, R. S., & Leijnse, M. Creating and detecting poor man’s Majorana bound states in interacting quantum dots. *Phys. Rev. B.* **106**, L201404 (2022).
- [30] Alvarez, G. The density matrix renormalization group for strongly correlated electron systems: A generic implementation. *Comput. Phys. Commun.* **180**, 1572-1578 (2009).
- [31] Nocera, A. & Alvarez, G. Spectral functions with the density matrix renormalization group: Krylov-space approach for correction vectors. *Phys. Rev. E* **94**, 053308 (2016).
- [32] Thomale, R., Rachel, S., and Schmitteckert, P. Tunneling spectra simulation of interacting Majorana wires. *Phys. Rev. B.* **88**, 161103(R) (2013).
- [33] Herbrych, J., Środa, M., Alvarez, G., Dagotto, E. Interaction-induced topological phase transition and Majorana edge states in low-dimensional orbital-selective Mott insulators. *Nat Commun.* **12**, 2955 (2021).
- [34] See the Supplemental Material for the detailed analytical calculations.
- [35] Dagotto, E., Moreo, A., Barnes, T. Hubbard model with one hole: Ground-state properties. *Phys. Rev. B.* **40**, 6721 (1989).
- [36] Dagotto, E., Fradkin, E., Moreo, A. SU(2) gauge invariance and order parameters in strongly coupled electronic systems. *Phys. Rev. B.* **38**, 2926(R) (1988).
- [37] Weithofer, L., Recher, P., & Schmidt, T. L. Electron transport in multiterminal networks of Majorana bound states. *Phys. Rev. B.* **90**, 205416 (2014).
- [38] Fornieri, A., Whitticar, A.M., Setiawan, F. et al. Evidence of topological superconductivity in planar Josephson junctions. *Nature* **569**, 89–92 (2019)
- [39] Zhou, T., Dartailh, M. C., Mayer, W., Han, J. E., Matos-Abiad, et al. Phase Control of Majorana Bound States in a Topological X Junction *Phys. Rev. Lett.* **124**, 137001 (2020).
- [40] White, S. R. Density matrix formulation for quantum renormalization groups. *Phys. Rev. Lett.* **69**, 2863 (1992).
- [41] Schollwöck, U. The density-matrix renormalization group. *Rev. Mod. Phys.* **77**, 259 (2005).
- [42] Pandey, B., Lin, L. F., Soni, R., Kaushal, N. et al. Prediction of exotic magnetic states in the alkali-metal quasi-one-dimensional iron selenide compound Na₂FeSe₂ *Phys. Rev. B.* **102**, 035149 (2020).